The *WISE* gamma-ray strip parametrization:
the nature of the gamma-ray Active Galactic Nuclei of Uncertain type

F. Massaro[1], R. D'Abrusco[2], G. Tosti[3,4], M. Ajello[1], D. Gasparrini[5], J. E. Grindlay[2] &
Howard A. Smith[2].

*SLAC National Laboratory and Kavli Institute for Particle Astrophysics and Cosmology,
2575 Sand Hill Road, Menlo Park, CA 94025*

Harvard - Smithsonian Astrophysical Observatory, 60 Garden Street, Cambridge, MA 02138

Dipartimento di Fisica, Università degli Studi di Perugia, 06123 Perugia, Italy

Istituto Nazionale di Fisica Nucleare, Sezione di Perugia, 06123 Perugia, Italy

ASI Science Data Center, ESRIN, I-00044 Frascati, Italy

ABSTRACT

Despite the large number of discoveries made recently by *Fermi*, the origins of the so called unidentified γ-ray sources remain unknown. The large number of these sources suggests that among them there could be a population that significantly contributes to the isotropic gamma-ray background and is therefore crucial to understand their nature. The first step toward a complete comprehension of the unidentified γ-ray source population is to identify those that can be associated with blazars, the most numerous class of extragalactic sources in the γ-ray sky. Recently, we discovered that blazars can be recognized and separated from other extragalactic sources using the infrared (IR) *WISE* satellite colors. The blazar population delineates a remarkable and distinctive region of the IR color-color space, the *WISE* blazar strip. In particular, the subregion delineated by the γ-ray emitting blazars is even narrower and we named it as the *WISE* Gamma-ray Strip (WGS). In this paper we parametrize the WGS on the basis of a single parameter s that we then use to determine if γ-ray Active Galactic Nuclei of the uncertain type (AGUs) detected by *Fermi* are consistent with the WGS and so can be considered blazar candidates. We find that 54 AGUs out of a set 60 analyzed have IR colors consistent with the WGS; only 6 AGUs are outliers. This result implies that a very high percentage (i.e., in this sample about 90%) of the AGUs detected by *Fermi* are indeed blazar candidates.

Subject headings: galaxies: active - galaxies: BL Lacertae objects - radiation mechanisms: non-thermal

1. Introduction

With the recent advent of the *Fermi* mission, the γ-ray astronomy is living a new golden age with several striking discoveries already performed during the first three years.

According to the second *Fermi* γ-ray LAT catalog (2FGL,), *Fermi* detected 1873 sources, 576 of which are still unidentified even if the localization of the γ-ray sources has significantly improved with respect to the past γ-ray missions. For this reason, despite the large number of new discoveries already achieved, the nature of the unidentified γ-ray sources is still an open question. This unsolved issue is extremely relevant for the origin of the isotropic gamma-ray background, since, given the large number of unidentified γ-ray sources, new classes of unknown extragalactic γ-ray sources that can significantly contribute to the isotropic gamma-ray background could be hidden.

On the other hand, the most detected γ-ray sources in the MeV-GeV energy range belong to the rarest class of active galactic nuclei, the blazars. They are an intriguing class of active galactic nuclei, characterized by non-thermal radiation emitted over the entire electromagnetic spectrum, and interpreted as arising from a relativistic jet closely aligned to the line of sight (see e.g.). Blazars come in two flavors: the BL Lac objects and the flat spectrum radio quasars, where the common discriminating criterion between the two classes is the equivalent width of the optical emission lines, traditionally weaker than $5\mathring{A}$ in the former rather than in the latter (;). In the following, we indicate the BL Lacs as BZBs and the Flat Spectrum radio quasars as BZQs, according to the ROMA-BZCAT nomenclature (;).

Recently, using the preliminary data release of the *WISE* infrared (IR) survey (), we discovered that IR color-color diagrams allows us to distinguish between extragalactic sources dominated by non-thermal emission, like blazars, and other classes of galaxies and/or active galactic nuclei (Massaro et al. 2011, hereinafter Paper I, see also Plotkin et al. 2011). In particular, the blazar population delineates a tight, distinct region of the IR color space, indicated as the *WISE* Blazar Strip (Paper I). The *WISE* Blazar Strip is a region in the 3D infrared color space delineated by the blazar population. This region is narrower when considering only the IR colors of the blazars that are detected in the γ-rays, indicated as the *WISE* gamma-ray strip (WGS, see , hereinafter Paper II). A 3D scatter plot of the *WISE* Blazar Strip and the subregion of the WGS are shown in the IR diagram of Figure 1, while

the [3.4]-[4.6]-[12] μm 2D projection is reported in Figure 2.

One of the major difficulties of the association procedures for the *Fermi* γ-ray sources with active galactic nuclei is that, due to the lack of radio and X-ray informations and to the large uncertainty on the γ-ray position, it is not always possible to recognize if there is a blazar candidate within the positional error region. Thus, the main aim of this paper is to build a parametrization of the WGS in order to verify whenever γ-ray sources have been associated to a counterpart that is a blazar candidate, being consistent with the WGS. In particular, we studied the *WISE* counterparts of the Active galactic nuclei of uncertain type (AGUs), defined according to the 2FGL and the 2LAC criteria (), and their consistency with the WGS. The AGUs are defined as the radio and/or X-ray counterparts of γ-ray sources associated to by the 2FGL Likelihood Ratio method, but without a good optical spectrum that enable their classification (). This paper is organized as follows. Section 2 describes the procedure adopted to parametrize the WGS. Section 3 we discuss on the consistency of the *WISE* counterparts of the AGU sample with the WGSwhile Section 4 describes the non-parametric analysis of the WGS based on the Kernel Density Estimation (KDE). In Section 5 we investigated possible selection effects that could affect our WGS parametrization. Our conclusions are discussed in Section 6.

2. The *WISE* gamma-ray strip parametrization

2.1. The sample selection

We use the sample of γ-ray emitting blazars already selected in Paper II to parametrize the WGS.

This sample was selected from the 2FGL, that contains 805 sources associated with a blazar: 435 BZBs and 370 BZQs respectively. However only 659 (347 BZBs and 312 BZQs) of these are listed and classified according to the criteria used in the ROMA-BZCAT (e.g.,). We excluded from our analysis all the blazars with a *Fermi* analysis flag, according to the 2FGL and the 2LAC (;).

In particular, 329 (164 BZBs and 165 BZQs) blazars, out of the original 659, lie in the portion of the sky reported in the *WISE* preliminary source catalog, but only 296 (143 BZBs and 153 BZQs) have a *WISE* counterpart within 2.4″ radius (see Paper I). To be more conservative, we excluded from our analysis 12 blazars (8 BZBs and 4 BZQs) with respect to the 296 blazars in sample selected in Paper II, because they have a 95% upper limit on the *WISE* magnitude at 22 μm. Then, we use this 2FB sample composed of the 284 blazars (135 BZBs and 149 BZQs) to build the WGS parametrization. We notice that all the selected

blazars also belong the 2LAC sample ().

According to the classification available in ROMA-BZCAT the blazars of uncertain type have been excluded from our analysis, while the BL Lac candidates have been considered as BZBs. More details about the 2FB sample and the source selections are given in Paper II.

Finally, we emphasize that our selection is based only on γ-ray blazars that belong to the ROMA-BZCAT because this is the largest catalog of blazars available in literature in which each source is spectroscopically classified at optical frequencies.

2.2. The *WISE* blazar associations

The IR color-color diagrams have been built using the archival *WISE* Preliminary Source Catalog, that covers $\sim 57\%$ of the sky [1] . The *WISE* mission mapped the sky at 3.4, 4.6, 12, and 22 μm in 2010 with an angular resolution of 6.1, 6.4, 6.5 & 12.0$''$ in the four bands, achieving 5σ point source sensitivities of 0.08, 0.11, 1 and 6 mJy respectively in unconfused regions on the ecliptic. All the *WISE* magnitudes are in the Vega system. In particular, the absolute (radial) differences between *WISE* source-peaks and "true" astrometric positions anywhere on the sky are no larger than ~ 0.50, 0.26, 0.26, and 1.4$''$ in the four *WISE* bands, respectively ()[2].

For our analysis, unless stated otherwise, we considered only *WISE* sources detected with a minimum signal-to-noise ratio of 7 in at least one band [3]. The positional coincidences of blazars in the observed *WISE* sky have been searched within a circular region of radius 2.4$''$. This corresponds to the combination of the error of 1$''$, assumed for the radio position reported in the ROMA-BZCAT () and taking into account of astrometric uncertainties in the *WISE* preliminary data, and the positional error of the fourth *WISE* band at 22μm (i.e., 1.4$''$) (see also Paper I). All the associations of the 2FB blazars with *WISE* sources are unique and no multiple matches have been found (see Papers I and II for more details). The chance probabilities of the *WISE* associations for the sources in the 2FGL and in the ROMA-BZCAT are reported in Paper II.

---

[1] wise2.ipac.caltech.edu/docs/release/prelim/preview.html

[2] wise2.ipac.caltech.edu/docs/release/prelim/expsup/sec2_3g.html

[3] We take the opportunity to correct here an error that appears in Paper II. The sources of the 2FB sample are detected with a minimum signal-to-noise ratio of 7 in at least one band rather than in all four bands as reported in Paper II.

2.3.   The *WISE* gamma-ray strip projections

We built the parametrization of the WGS considering only the sources in the 2FB sample (see Section 2.1) and using the three different 2D projections of the WGS delineated in the [3.4]-[4.6]-[12] μm, [4.6]-[12]-[22] μm, [3.4]-[4.6]-[22] μm color-color planes. In each color-color 2D projection we determined the smaller irregular quadrilateral containing at least 95% of the blazars in the 2FB sample considering their position within error (see also Section 2.4 for more details). The irregular quadrilateral defining the WGS subregions have been drawn by hand. The KDE analysis has been used to verify, *a posteriori*, that the hand-drawn boundaries of the WGS are in agreement with the sharp decline in density of WGS sources, as evaluated by this non parametric method **(see Section 4 for more details)**. This WGS modeling has been developed separately for the BZBs and the BZQs, and for all their three 2D projections.

The [3.4]-[4.6]-[12] μm, [4.6]-[12]-[22] μm and [3.4]-[4.6]-[12]-[22] μm 2D projections of the WGS for the BZB and the BZQ populations are shown in Figure 3, Figure 4, Figure 5 and Figure 6), respectively.

In the following we also report the boundaries chosen for our WGS parametrization. For the BZB projections the extremal points of the WGS have coordinates: P_1=(2.01,0.37), P_2=(3.30,1.17), P_3=(2.59,1.20), P_4=(1.52,0.51) in Figure 3, P_1=(2.20,1.65), P_2=(2.72,2.57), P_3=(2.29,3.30), P_4=(1.20,1.96), in Figure 5 (upper panel), while P_1=(2.05,0.33), P_2=(2.83,1.07), P_3=(2.28,1.21), P_4=(1.20,0.73), in Figure 5 (lower panel).

On the other hand, for the BZQ projections the extremal points of the WGS have coordinates: P_1=(2.90,0.85), P_2=(3.81,1.17), P_3=(3.29,1.67), P_4=(2.29,1.08) in Figure 4, P_1=(2.25,2.22), P_2=(3.04,3.05), P_3=(2.67,3.70), P_4=(1.68,2.85), in Figure 6 (upper panel), while P_1=(2.48,0.78), P_2=(3.05,1.17), P_3=(2.55,1.50), P_4=(1.72,1.12), in Figure 6 (lower panel).

2.4.   The strip parameter s

To illustrate the WGS parametrization we consider the schematic case of the first projection: [3.4]-[4.6], [4.6]-[12], hereinafter c_1-c_2 with the correspondent errors σ_1 and σ_2, respectively (see Figure 7).

Based on the *WISE* source location in the c_1-c_2 diagram we can distinguish 5 types of objects. Each source, given its IR colors, corresponds to a single point in each 2D color-color projection of the WGS. However, including the errors on both axes, it is represented by a

cross with 4 *extremal points*, calculated considering the $\pm 1\sigma$ error on each color. Then, we can define five different type of sources, according to the schematic view shown in Figure 7:

- *type 4*: sources with all the extremal points within the WGS projection;

- *type 3*: sources for which only 3 extremal points lie within the region of the WGS;

- *type 2*: sources with only two extremal points consistent with the WGS;

- *type 1*: sources with only a single extremal point associated with the WGS;

- *type 0*: sources without extremal points of the error cross on the WGS.

We can assign to each type of source a *discrete strip parameter d* ranging between 0 and 1, according to the scheme illustrated in Figure 7. For example, in the case of the c_1-c_2 projection of the WGS, we assign to type 4 sources a value $d_{12}=1$, while source of type 0 corresponds to $d_{12}=0$. For the same 2D projection, the intermediate values have been assigned as follows: type 3 have $d_{12}=0.75$, type 2 have $d_{12}=0.5$ and type 1 $d_{12}=0.25$.

On the same c_1-c_2 diagram, we also assign a *weight strip parameter w_{12}* to each value of the d_{12} parameter defined as: $w_{12}= (\sigma_1\,\sigma_2)^{-1/2}$, proportional to the area of the ellipse described by the error bars of each point (see inset of Figure 7 for more details). Then, we define the *continuos strip parameter s_{12}* as:

$$s_{12} = d_{12}\,w_{12}. \qquad (1)$$

We note that the parameter w_{12} has been chosen to take into account the different errors on both axes when comparing two sources that might belong to the same type. It also allow us to make the s_{12} continuos rather than discrete as d_{12}.

We repeated the entire procedure described above for each 2D projection of the WGS: c_1-c_2, c_2-c_3 and c_1-c_3, generating the values of the continuos strip parameters s_{12}, s_{23}, s_{13}, respectively. Then, all these values of the strip parameters for three different 2D projections have been combined together to define an unique *total strip parameter s*. The *total strip parameter* is the geometric average of the s values of each 2D projection:

$$s = (s_{12}\,s_{23}\,s_{13})^{1/3}. \qquad (2)$$

We emphasize that sources that lie outside of the WGS in at least one of its 2D projection have one of the correspondent s_{12}, s_{23}, s_{13} parameter equal to zero and consequently the total s value is null as well. This occurs because the discrete d parameter is zero for sources outside the WGS (see Figure 7).

We divided all the s parameters for the maximum s values of the BZBs and BZQs that lie on the WGS to re-normalize s in the range 0 and 1. This re-normalization can be applied to the s values of all the *WISE* sources, because those outside the WGS will have s null by definition.

The s parameter represents an estimate of the *distance*, in the IR colors parameter space and weighted with the errors on each axes, between the WGS and a generic *WISE* source, that could potentially belong to it; this s parameter is different from zero only in the case in which the all color error bars of a *WISE* source are consistent with the WGS. Therefore these s values can be used to rank each IR *WISE* source according to their *association* to the WGS.

Finally, we note that to test if a generic *WISE* source has IR colors consistent with the BZBs or with the BZQs subregion of the WGS, the total strip parameters are indicated as s_b and s_q, respectively. We introduced the above divisions for the s parameters because in future works this allow us to verify if a generic *WISE* source is more consistent to be a BZB or a BZQ, enabling a classification for new IR sources that could lie on the WGSbeing γ-ray blazar candidates.

2.5. The s parameter distributions

We considered a sample composed of all the *WISE* sources lying in two circular regions of 1 deg radius, centered at high and low Galactic latitude b, with the center coordinates of $(l, b)=(255,-55)$ deg and $(l, b)=(338,-1)$ deg, respectively. These sources do not have upper limits on their *WISE* magnitude values and are detected with a signal to noise ratio > 7 in at least one band as for the blazars in the 2FB sample.

We calculated the s parameters for all the 11599 generic IR *WISE* sources. This analysis provides an estimate of the probability to find a generic *WISE* source in the sky with a particular value of s_b and/or s_q. We perform this analysis considering the distinction between the two blazar classes (i.e., BZBs and BZQs), The distributions of the s_b and s_q parameters for the BZBs and the BZQs that lie on the WGS in comparison with the generic IR *WISE* sources are shown in Figure 8 and in Figure 9, respectively.

From the distributions of the s_b and s_q parameters for the generic IR *WISE* sources, we note that 99.9% of them have $s_b <0.24$ and $s_q <0.38$. Then, for the BZBs in the 2FB sample only 6 sources out of 135 have $s_b < 0.24$, and in the case of the BZQs only 33 sources out of 149 show s_q values lower than 0.38. We also note that 99.0% of the generic IR *WISE* sources have $s_b <0.10$ and only 2 BZBs are below this value, while 97.2% of the generic IR

WISE sources together with only 5 BZQs out of 149 have $s_q < 0.14$. Finally, on the basis of the above s distributions we define the *outliers* of the WGS, *WISE* sources that have values of $s_b < 0.10$ or $s_q < 0.14$.

We recognize that the above choice of the s_b and s_q thresholds are extremely conservative. This choice has been made on the basis of the actual sky coverage of the *WISE* preliminary data release. At the present status of our analysis we are not able to investigate the IR emission of all the blazars that are listed in the 2FGL, and the 2FB sample used to build the WGS parametrization is small with respect to how it will be available when the *WISE* full archive will be released. Consequently, regarding the choice of the threshold values for the s parameters, we preferred the efficiency to the completeness of our method selecting the s limiting values from their distributions in low galactic latitude regions, even if this choice could increase the possible contamination of the WGS. A deeper investigation of this problem will be considered in future as an *a posteriori* analysis of WGS parametrization. In particular, when the *WISE* full release will be available, we will improve our method taking into account of the IR source density at different galactic latitudes and of the varying depth of the exposure for the *WISE* observations.

3. The AGU counterparts on the WGS

We considered the sample composed of all the AGUs already classified in the analysis of the 2FGL and the 2LAC (;). According to the 2FGL, the AGUs could be all blazar candidates without a good optical spectrum or without an optical spectrum at all (;).

We selected the AGUs that lie in the portion of the sky surveyed by *WISE* during the first year, corresponding to 148 *Fermi* sources. Then, we excluded from our analysis all the AGUs with a *Fermi* analysis flag, according to the 2FGL and the 2LAC.

The association between each AGU counterpart and the *WISE* sources have been evaluated on the basis of the same criterion chosen for the blazars on the *WISE* Blazar Strip (see Section 2.2 and Paper I for more details), considering the position of the radio counterpart for each AGU as reported in the 2FGL and/or in the 2LAC. There are 60 AGUs out of 148 for which there is a unique association with a *WISE* source (see Section 3) within the usual region of $2.4''$ radius and with a chance probability of 0.008, estimated adopting the method described in Maselli et al. (2010) (see also , and Paper I) and without upper limits on the *WISE* magnitudes within the *WISE* preliminary data release.

Subsequently, we used the IR colors of the AGU counterparts, as associated in the 2LAC, to verify if the *WISE* counterparts of the γ-ray sources in the 60 AGU sample lie on

the WGS, evaluating their s values following the procedure described in Section 2.

We found that 6 outliers do not belong to the WGS out of 60 AGUs, according to the inclusion based on the threshold values of $s_b < 0.10$ or $s_q < 0.14$. With this analysis on the 60 AGU sample, we have been able to check if the association provided by the 2FGL corresponds to a blazar lying on the WGS.

Finally, we estimated the IR spectral index α_{IR} using the [3.4]-[4.6] μm color according to Eq. (1) of Paper II, and we evaluated the correlation between α_{IR} and the spectral index of the associated 2FGL source α_γ. We found a linear correlation between α_{IR} and α_γ for the 54 AGU that lie on the WGS, with a correlation coefficient $\rho = 0.56$ and a chance probability of 8.96×10^{-6} and a slope $m = 0.30 \pm 0.06$, that is consistent with that of the WGS blazars ($\rho = 0.68$, $m = 0.36 \pm 0.02$, see Paper II) within one sigma (see Figure 10). On the other hand, the 6 outliers have a weaker linear correlation between the two spectral indices then the previous sample with $\rho = 0.40$ (chance probability of 0.08) and $m = 0.12 \pm 0.07$, different from that of the blazars on the WGS (see Figure 10). Finally, in Table 1 and in Table 2 we report the colors, the IR spectral indices and the s parameters together with the 2FGL name and the *WISE* and the counterpart names of each AGU analyzed. The class of each AGU as derived from the 2LAC analysis is also indicated ().

4. An independent non-parametric analysis: the kernel density estimation

To test our analysis, we also performed a statistical investigation based on an independent non-parametric method as the KDE technique as already proposed in Paper I (see also ; , and reference therein). The KDE method provides an effective way of estimating the probability function of a multivariate distribution and do not require any assumption about the shape of the "parent" distributions. In Figure 11, the isodensity contours drawn from the KDE density probabilities and associated with different levels of density are plotted for the blazars of the WGS in its [3.4]-[4.6]-[12]-[22] μm 2D projection.

Consequently, for a generic source in the *WISE* archive we can provide an estimate of the probability π_{kde} that a blazar of the WGS has the same IR colors, this is a surrogate of the probability that a *WISE* source is consistent with the WGS. In Figure 11, we also show the AGU counterparts with respect to the isodensity contours of the WGS, to highlight the outliers. We also report in Table 1 and in Table 2, the value of π_{kde} for each AGU analyzed.

Finally, we note that there are some AGUs for which the KDE analysis suggests that the source is not consistent with the WGS, even if the parametric method indicates it as a possible candidate. The reason for this to happen is that, as previously mentioned, the KDE

method does not take into account the errors on the IR colors. As a consequence, sources far from the WGS but with large errors could be associated to low density values, as calculated by the KDE method, and discarded. However, our parametrization of the WGS allows us to take into account the errors on the *WISE* colors and to consider also this type of sources. We emphasize that all the sources that the WGS parametrization indicates as outliers have also π_{kde} typically lower than $\sim 1\%$ of being consistent with the WGS.

5. An analysis of possible selection effects

In future, thanks to the developed WGS parametrization, we will be also able to investigate if there are selection effects that could affect our analysis as for example driving the WGS thickness. At the current stage of our study, we are able to estimate when a generic *WISE* sources in consistent with the WGS itself that is a necessary tool to compare different samples for future investigations; Thanks to the parametrization developed we will be also able to verify if there are IR blazars that belong to the WGS but are not detected in γ-rays, and which could be the physical conditions if this occurs.

We remark that the link between the IR and the γ-ray properties of blazars, is mainly due to the relation between the blazar spectral shape in the IR and in the γ-rays. To evaluate if selection effects due to flux limits in the selected sample could affect our WGS description we performed the following tests. We restricted our analysis to the bright *WISE* blazars with IR magnitudes in the ranges: $m_1 \leq 13.5$, $m_2 \leq 12$, $m_3 \leq 11$, $m_4 \leq 7.5$, that belong to both the *WISE* Blazar strip and to the WGS, and we found that a difference in their thickness is still evident (see Figure 12 for the standard 2D projection in [3.4]-[4.6]-[12] μm color diagram). This plot suggests that the origin of the WGS is not due to a selection of bright IR blazars.

We also compared the WGS as formed by the blazars present in the 2FGL and those detected in the first *Fermi* LAT catalog (1FGL) (), and again we did not find any clear difference between the WGS drawn with the bright or the faint γ-ray blazars. This again suggests that the relation between the WGS and the γ-ray detectability is related to the blazar spectral shape (see Figure 13 for the standard 2D projection in [3.4]-[4.6]-[12] μm color diagram). On the basis of the WGS parametrization presented in this paper, the above issues will be deeply addressed in future works, after the full release of the *WISE* all-sky survey.

6.   Summary and Discussion

On the basis of the recent results on the characterization of the IR colors of blazars provided by *WISE* (Paper I) and on the comparison with their γ-ray emission (Paper II), we developed a method based the *WISE* Blazar Strip to identify blazar counterparts of γ-ray sources.

We developed a method to parametrize the WGS in the 3D color diagrams based on its 2D projections. This method is characterized by the use a continuos parameter s, in the range $0 - 1$, that takes into account of the errors of all the IR colors and provides clues on the position of a generic *WISE* source relative to the WGS in the 3D color parameter space. High values of the s parameters are associated to sources that lie inside the WGS (as the γ-ray blazar population of the 2FB sample). The WGS has been parametrized in two subregions, the first containing the BZBs while the other with the BZQs although in the present work we are only interest in searching for blazar counterparts that lie on the WGS.

We applied our parametrization to the sample of the AGUs selected from the 2FGL and the 2LAC. We found that there are 148 AGUs that can be analyzed within the footprint of the *WISE* preliminary source catalog. However, according to our association procedure (see Secton 2.2) only 60 AGUs have a unique *WISE* counterpart without any upper limit on the *WISE* magnitude values.

Then, we calculated the distributions of their s parameter and found that 54 out of 60 AGUs analyzed are consistent with the WGS, corresponding to the 90% of the γ-ray counterparts analyzed while the remaining 6 AGU counterparts are outliers of the WGS. In particular, for the 54 AGUs that are consistent with the WGS we also found that the correlation between the α_{IR} and α_γ is in agreement with that found for the blazars that constitute the WGS itself while the same correlation for the 6 outliers is inconsistent with it.

We also applied the KDE non-parametric test to obtain the probability that an AGU counterpart belong to the WGS and we found consistent results with our parametrization (see Section 4 for more details).

In addition, an extensive investigation of all the unidentified γ-ray sources in the 2FGL that fall in the area of the sky where the *WISE* preliminary data have been already released will be provided in a forthcoming paper (). Searching for blazar candidates within the unidentified γ-ray source sample could potentially leading to the discovery new class of γ-ray emitting sources.

Further improvements of the WGS parametrization will be also possible in the future,

when the whole *WISE* catalog will be available and this parametric method would be calibrated at different b values not only to look for counterparts of γ-ray sources but also to search for new blazar candidates all over the sky ().

REFERENCES

Abdo, A. A. et al. 2010b ApJS 188 405

Abdo, A. A. et al. ApJS submitted http://arxiv.org/abs/1108.1435

Ackermann, M. et al. 2011a ApJ, 743, 171

Blandford, R. D., Rees, M. J., 1978, PROC. "Pittsburgh Conference on BL Lac objects", 328

Cutri, R. M. 2011, wise.rept, 1

D'Abrusco, R., Longo, G., Walton, N. A. 2009 MNRAS , 396, 223

---

[4]www.star.bris.ac.uk/∼mbt/topcat/

D'Abrusco, R., Massaro, F., Ajello, M., Grindlay, J. E., Smith, Howard A. & Tosti, G. 2012 ApJ accepted

Laurino, O. & D'Abrusco 2011 MNRAS in press

Maselli, A., Massaro, E., Nesci, R., Sclavi, S., Rossi, C., Giommi, P. 2010 A&A, 512A, 74

Maselli, A., Cusumano, G., Massaro, E., Segreto, A., La Parola, V., Tramacere, A., Donnarumma, I. 2011A&A 531, 153

Massaro, F., Tramacere, A., Cavaliere, A., Perri, M., Giommi, P. 2008 A&A, 478, 395

Massaro, E., Giommi, P., Leto, C., Marchegiani, P., Maselli, A., Perri, M., Piranomonte, S., Sclavi, S. 2009 A&A, 495, 691

Massaro, E., Giommi, P., Leto, C., Marchegiani, P., Maselli, A., Perri, M., Piranomonte, S., Sclavi, S. 2010 arxiv.org/abs/1006.0922

Massaro, F., D'Abrusco, R., Ajello, M., Grindlay, J. E. & Smith, H. A. 2011 ApJ, 740L, 48

Massaro, F., D'Abrusco, R., Tosti, G., Ajello, M., Paggi, A., Gasparrini, D., 2012 ApJ submitted

Massaro, F., D'Abrusco, R., Tosti, G. et al. 2012 in preparation

Plotkin, R. M., Anderson, S. F., Brandt, M. N., Markoff, S., Shemmer, O., Wu, J. 2011 ApJL accepted arXiv:1112.5162

Stickel, M., Padovani, P., Urry, C. M., Fried, J. W., Kuehr, H. 1991 ApJ, 374, 431

Stocke et al. 1991, ApJS, 76, 813

Taylor, M. B. 2005, ASP Conf. Ser., 347, 29

Wright E. L., et al. 2010 AJ, 140, 1868

Table 1: The parameters of the *WISE* counterparts for the outliers of the WGS.

2FGL name	*WISE* name	Name	Class	c_1	σ_1	c_2	σ_2	c_3	σ_3	α_{IR}	$\sigma_{\alpha_{IR}}$	s_b	s_q	π_{kde}
2FGLJ0532.5-7223	J053344.71-721623.3	PMN J0533-7216	-	1.042	0.088	1.884	0.286	3.485	0.457	1.175	0.257	0.0	0.0	5.963e-6
2FGLJ0602.3+5315	J060200.44+531600.2	GB6 J0601+5315	HSP	0.274	0.032	1.707	0.058	2.074	0.174	-1.05	0.093	0.0	0.0	4.18e-5
2FGLJ0605.0+0001	J060458.42+000043.2	GB6 J0604+0000	-	0.285	0.034	1.218	0.089	1.836	0.431	-1.02	0.099	0.0	0.0	2.09e-9
2FGLJ1304.1-2415	J130342.56-241442.1	1RXS 130343.6-241506	HSP	0.195	0.041	2.506	0.073	1.996	0.269	-1.28	0.118	0.0	0.0	4.49e-9
2FGLJ1753.8-5012	J175338.55-501513.7	PMN J1753-5015	-	0.663	0.050	2.647	0.057	2.341	0.122	0.071	0.147	0.0	0.0	0.003
2FGLJ1936.9+8402	J193739.76+835628.9	6C B194425+834912	-	1.334	0.147	2.938	0.232	2.714	0.581	2.030	0.431	0.0	0.06	0.01

Col. (1) Source name reported in the 2FGL ().
Col. (2) Source name reported in the *WISE* preliminary data release.
Col. (3) Source name as reported in the 2LAC ().
Col. (4) Source class as reported in the 2LAC: high-synchrotron-peaked blazar (HSP), intermediated-synchrotron-peaked blazar (ISP), intermediated-synchrotron-peaked blazar (LSP).
Col. (5) IR color $c_1 = [3.4]$-$[4.6]$ μm.
Col. (6) Error σ_1 on c_1.
Col. (7) IR color $c_2 = [4.6]$-$[12]$ μm.
Col. (8) Error σ_2 on c_1.
Col. (9) IR color $c_3 = [12]$-$[22]$ μm.
Col. (10) Error σ_3 on c_3.
Col. (11) IR spectral index α_{IR}.
Col. (12) Error on α_{IR}.
Col. (13,14) s_b and s_q values.
Col. (15) Probability derived from the KDE analysis π_{kde}.

Table 2: The parameters of the *WISE* counterparts for the blazar candidates.

2FGL name	WISE name	Name	Class	c_1	σ_1	c_2	σ_2	c_3	σ_3	α_{IR}	$\sigma_{\alpha_{IR}}$	s_b	s_q	π_{kde}
2FGLJ0156.4+3909	J015631.40+391430.5	MG4 J015630+3913	-	1.167	0.042	2.731	0.063	2.344	0.196	1.541	0.124	0.273	0.355	0.28
2FGLJ0248.6+8440	J024948.29+843556.9	NVSS J024948+843556	-	0.958	0.036	2.654	0.039	2.062	0.098	0.927	0.105	0.548	0.475	0.41
2FGLJ0253.4+3218	J025333.64+321720.4	MG3 J025334+3217	-	1.163	0.043	2.954	0.060	2.518	0.117	1.529	0.126	0.317	0.428	0.60
2FGLJ0309.3-0743	J030943.22-074427.5	NVSS J030943-074427	HSP	0.728	0.036	2.128	0.071	2.037	0.248	0.260	0.106	0.327	0.109	0.18
2FGLJ0332.5-1118	J033223.25-111950.6	NVSS J033223-111951	HSP	0.977	0.033	2.652	0.033	2.194	0.050	0.986	0.099	0.739	0.748	0.43
2FGLJ0333.7+2918	J033349.00+291631.6	TXS 0330+291	ISP	0.820	0.036	2.096	0.048	2.106	0.134	0.525	0.105	0.460	0.0	0.09
2FGLJ0424.3-5332	J042504.26-533158.3	PMN J0425-5331	ISP	0.993	0.032	2.614	0.031	2.065	0.050	1.032	0.095	0.762	0.733	0.41
2FGLJ0438.8-4521	J043900.84-452222.2	PKS 0437-454	LSP	1.189	0.037	3.111	0.041	2.393	0.087	1.605	0.109	0.287	0.559	0.74
2FGLJ0440.1-3211	J043933.88-321009.8	PKS 0437-322	LSP	0.757	0.069	2.701	0.148	2.519	0.422	0.344	0.201	0.114	0.078	4.12e-4
2FGLJ0440.4+1433	J044021.13+143756.5	TXS 0437+145	-	1.234	0.048	3.020	0.068	2.489	0.163	1.737	0.140	0.0	0.354	0.43
2FGLJ0456.5-2658	J045617.36+270220.7	MG2 J045613+2702	-	1.122	0.043	2.903	0.061	2.297	0.159	1.409	0.128	0.377	0.381	1.00
2FGLJ0505.9+6116	J050558.78+611335.6	NVSS J050558+611336	HSP	0.766	0.041	1.948	0.085	1.961	0.347	0.371	0.119	0.211	0.0	0.11
2FGLJ0508.1-1936	J050818.99-193556.0	PMN J0508-1936	-	1.048	0.070	2.901	0.151	2.455	0.474	1.190	0.205	0.128	0.150	0.59
2FGLJ0525.5-6011	J052542.42-601340.8	SUMSS J052542-601341	HSP	0.718	0.044	2.268	0.125	2.577	0.369	0.231	0.129	0.163	0.093	0.01
2FGLJ0526.8+6326	J052606.71+631729.0	GB6 J0526+6317	-	0.996	0.045	2.709	0.077	1.656	0.349	1.041	0.134	0.193	0.140	0.02
2FGLJ0532.0-4826	J053158.61-482736.1	PMN J0531-4827	LSP	0.899	0.031	2.492	0.029	1.998	0.039	0.755	0.090	0.862	0.457	0.37
2FGLJ0537.7-5716	J053748.95-571830.0	SUMSS J053748-571828	ISP	0.857	0.033	2.348	0.041	2.131	0.112	0.636	0.096	0.530	0.281	0.17
2FGLJ0538.5-3909	J053810.35-390842.5	1RXS 053810.0-390839	HSP	0.621	0.041	2.032	0.118	2.003	0.492	-0.050	0.119	0.194	0.061	0.13
2FGLJ0604.2-4817	J060408.61-481724.9	1ES 0602-482	HSP	0.666	0.036	1.943	0.085	2.497	0.224	0.080	0.106	0.233	0.0	0.006
2FGLJ0609.4-0248	J060915.06-024754.6	NVSS J060915-024754	HSP	0.855	0.036	2.218	0.064	1.716	0.321	0.627	0.107	0.284	0.130	0.21
2FGLJ0621.9+3750	J062157.63+375057.4	GB6 J0621+3750	-	1.204	0.053	3.096	0.070	2.396	0.161	1.646	0.155	0.164	0.339	0.68
2FGLJ0703.1-3912	J070312.64-391418.7	NVSS J070312-391418	ISP	0.962	0.036	2.602	0.04	2.025	0.105	0.942	0.105	0.531	0.436	0.40
2FGLJ0706.5-7741	J070651.32-774137.1	NVSS J070651+774137	ISP	0.919	0.033	2.489	0.034	1.904	0.079	0.816	0.097	0.628	0.264	0.31
2FGLJ0734.2-7706	J073443.42-771114.1	PKS 0736-770	LSP	1.128	0.041	3.165	0.052	2.463	0.134	1.427	0.120	0.334	0.435	0.59
2FGLJ0823.0+4041	J082257.55+404149.8	B3 0819+408	LSP	1.177	0.037	2.963	0.041	2.293	0.072	1.570	0.109	0.512	0.596	0.70
2FGLJ0856.0+7136	J085654.85+714623.4	GB6 J0856+7146	LSP	1.152	0.036	3.007	0.04	2.442	0.071	1.494	0.107	0.450	0.608	0.88
2FGLJ1021.6+8021	J102202.09+802349.9	WN B1016.6+8038	-	0.945	0.046	2.741	0.083	2.534	0.212	0.889	0.134	0.278	0.263	0.06
2FGLJ1029.9-7437	J103122.15-744157.0	S5 1027+74	ISP	0.507	0.032	2.269	0.035	2.210	0.063	-0.383	0.094	0.387	0.0	0.01
2FGLJ1304.3-4353	J130421.02-435310.1	1RXS 130421.2-435308	HSP	0.869	0.034	2.268	0.032	1.921	0.053	0.671	0.099	0.727	0.305	0.30
2FGLJ1351.3-2909	J135146.86-291217.5	PKS 1348-289	-	1.077	0.040	2.885	0.059	2.49	0.137	1.275	0.117	0.392	0.415	0.62
2FGLJ1406.2-2510	J140609.61-250808.6	NVSS J140609-250808	-	0.868	0.040	2.461	0.067	2.110	0.228	0.668	0.117	0.333	0.209	0.24
2FGLJ1407.5-4257	J140739.73-430231.9	CGRaBS J1407-4302	LSP	0.948	0.043	2.724	0.066	2.429	0.149	0.901	0.125	0.377	0.365	0.12
2FGLJ1416.0+1323	J141558.82+132023.8	PKS B1413+135	LSP	1.355	0.031	2.897	0.030	2.264	0.038	2.089	0.093	0.0	0.766	0.03
2FGLJ1416.3-2415	J141612.18-241813.4	NVSS J141612-241812	HSP	0.464	0.036	1.702	0.093	2.293	0.277	-0.508	0.106	0.141	0.0	0.003
2FGLJ1419.4-7730	J141900.31+773228.8	1RXS 141901.8+773229	HSP	0.652	0.041	2.013	0.116	2.206	0.493	0.039	0.119	0.195	0.0	0.09
2FGLJ1419.4-0835	J141922.56-083832.1	NVSS J141922-083830	LSP	1.121	0.037	2.885	0.045	2.26	0.091	1.406	0.109	0.528	0.534	0.92
2FGLJ1421.1-1117	J142100.15-111820.1	PMN J1420-1118	-	1.080	0.056	2.714	0.122	2.449	0.318	1.286	0.165	0.208	0.207	0.39
2FGLJ1518.2-2733	J151803.60-273131.0	TXS 1515-273	-	0.692	0.033	2.190	0.044	2.127	0.097	0.153	0.098	0.539	0.180	0.11
2FGLJ1553.2-2424	J155331.63-242205.7	PKS 1550-242	-	1.100	0.037	3.058	0.045	2.402	0.090	1.342	0.109	0.506	0.536	0.85
2FGLJ1558.3+8513	J160031.78+850949.2	WN B1609.6+8517	LSP	0.868	0.034	2.301	0.043	2.078	0.132	0.668	0.100	0.487	0.234	0.21
2FGLJ1558.6-7039	J155736.14-704027.1	PKS 1552-705	-	0.906	0.082	3.042	0.151	2.594	0.354	0.776	0.241	0.0	0.142	0.01
2FGLJ1725.1-7714	J172350.85-771349.9	PKS 1716-771	-	1.038	0.033	2.769	0.040	2.254	0.092	1.164	0.097	0.568	0.575	0.72
2FGLJ1759.2-4819	J175858.45-482112.6	PMN J1758-4820	-	0.978	0.038	2.609	0.036	2.194	0.057	0.986	0.112	0.655	0.635	0.39
2FGLJ1816.7-4942	J181656.00-494344.0	PMN J1816-4943	-	1.076	0.051	2.868	0.066	2.048	0.213	1.272	0.149	0.274	0.320	0.32
2FGLJ1818.7+2138	J181905.22+213234.0	MG2 J181902+2132	-	0.932	0.038	2.464	0.055	2.098	0.187	0.851	0.111	0.386	0.261	0.31
2FGLJ1825.1-5231	J182513.82-523057.7	PKS 1821-525	-	1.074	0.034	2.864	0.034	2.220	0.067	1.269	0.099	0.658	0.666	0.87
2FGLJ1829.1+2725	J182913.97+272902.9	87GB 182712.0+272717	-	0.776	0.042	2.796	0.059	2.424	0.157	0.400	0.123	0.0	0.147	8.65e-4
2FGLJ1830.0+1325	J183000.76+132414.4	MG1 J183001+1323	-	1.015	0.043	2.631	0.047	2.199	0.122	1.094	0.126	0.451	0.457	0.46
2FGLJ1858.1-2510	J185819.07-251050.5	PMN J1858-2511	-	1.068	0.106	3.183	0.100	2.654	0.179	1.248	0.310	0.123	0.231	0.14
2FGLJ1913.4-4440	J191401.88+443832.5	1RXS 191401.9+443849	HSP	0.737	0.039	2.256	0.081	1.823	0.400	0.283	0.115	0.249	0.125	0.20
2FGLJ1940.8-6213	J194121.77-621120.8	PKS 1936-623	-	1.330	0.036	2.860	0.043	2.312	0.092	2.018	0.107	0.0	0.542	0.04
2FGLJ1941.6+7218	J194127.01+722142.2	87GB 194202.1+721428	-	1.216	0.080	3.383	0.124	2.659	0.271	1.684	0.236	0.0	0.194	0.13
2FGLJ1959.6-2931	J200016.96-293026.2	PMN J2000-2931	-	0.825	0.049	2.398	0.094	2.298	0.304	0.539	0.144	0.241	0.147	0.04
2FGLJ2103.6-6236	J210338.37-623225.5	PMN J2103-6232	HSP	0.828	0.033	2.312	0.037	1.753	0.132	0.548	0.096	0.516	0.217	0.26

Col. (1) Source name reported in the 2FGL ().
Col. (2) Source name reported in the *WISE* preliminary data release.
Col. (3) Source name as reported in the 2LAC ().
Col. (4) Source class as reported in the 2LAC: high-synchrotron-peaked blazar (HSP), intermediated-synchrotron-peaked blazar (ISP), intermediated-synchrotron-peaked blazar (LSP).
Col. (5) IR color c_1 = [3.4]-[4.6] μm.
Col. (6) Error σ_1 on c_1.
Col. (7) IR color c_2 = [4.6]-[12] μm.
Col. (8) Error σ_2 on c_1.
Col. (9) IR color c_3 = [12]-[22] μm.
Col. (10) Error σ_3 on c_3.
Col. (11) IR spectral index α_{IR}.
Col. (12) Error on α_{IR}.
Col. (13,14) s_b and s_q values.
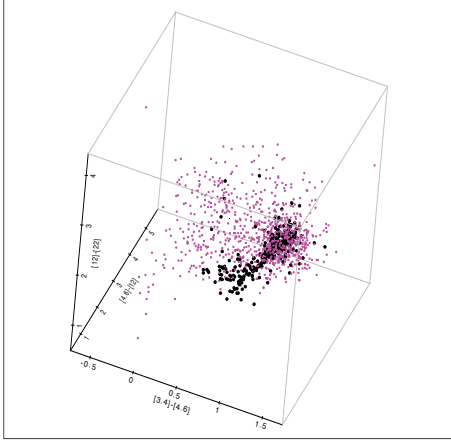Col. (15) Probability derived from the KDE analysis π_{kde}.

Fig. 1.— The 3D representation of the *WISE* Blazar Strip (blazars are indicated in magenta) and the subregion of the WGS (γ-ray emitting blazars are indicated in black) in the IR colors built with the magnitudes in the *WISE* bands at [3.4]-[4.6]-[12]-[22] μm.
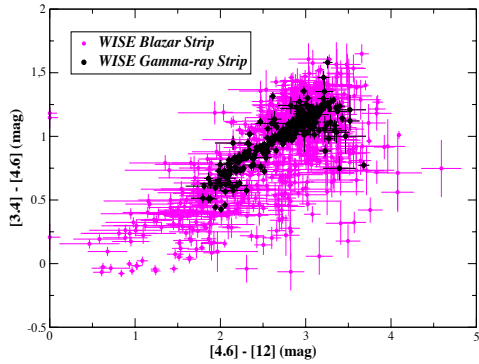

Fig. 2.— The 2D projection of the *WISE* Blazar Strip (blazars are in magenta) and the subregion of the WGS (γ-ray emitting blazars are in black) in the IR color diagram [3.4]-[4.6]-[12] μm.
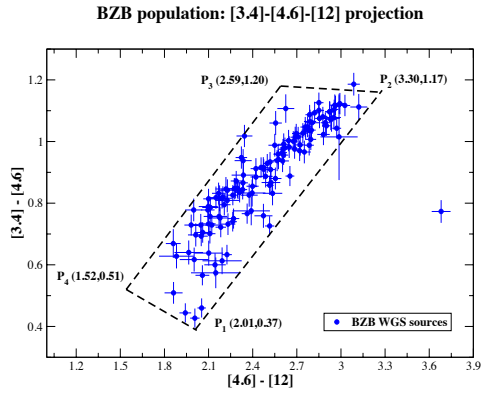
Fig. 3.— The [3.4]-[4.6]-[12] μm 2D projection of the WGS in the subregion of the BZB population is shown.
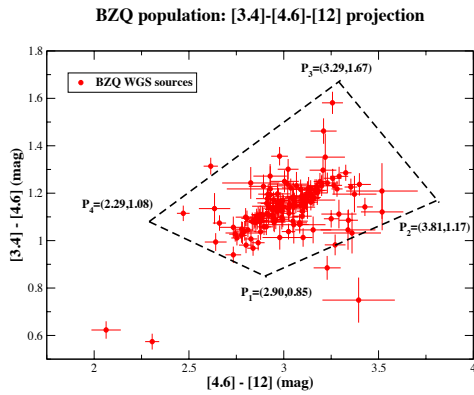
Fig. 4.— Same of Figure 4 but for the case of the BZQ population.
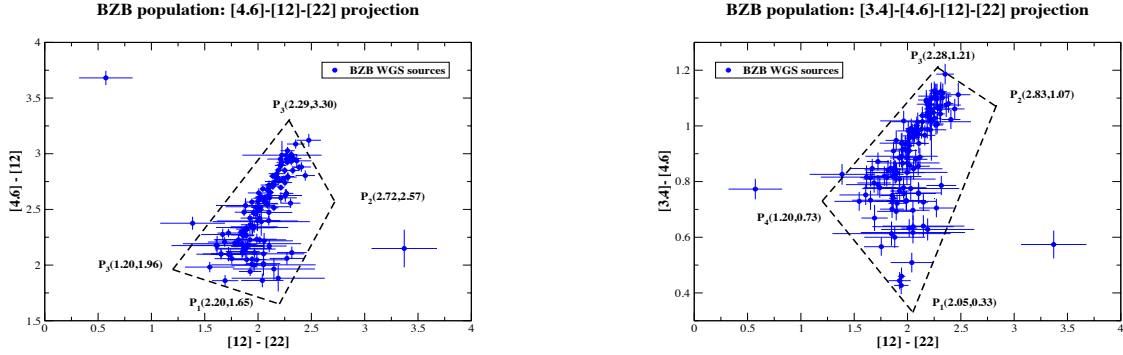
Fig. 5.— Same of Figure 3 for the case of the BZB population on the WGS in the two remaining different color-color projections.
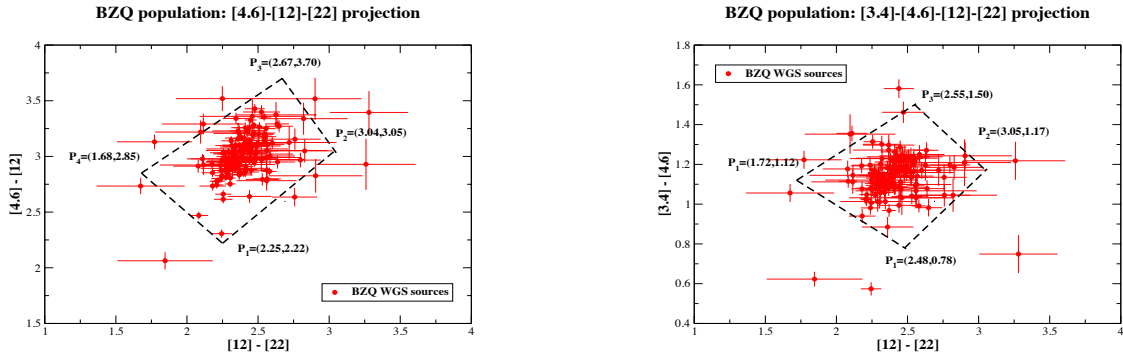
Fig. 6.— Same of Figure 4 for the case of the BZQ population on the WGS in the two remaining different color-color projections.
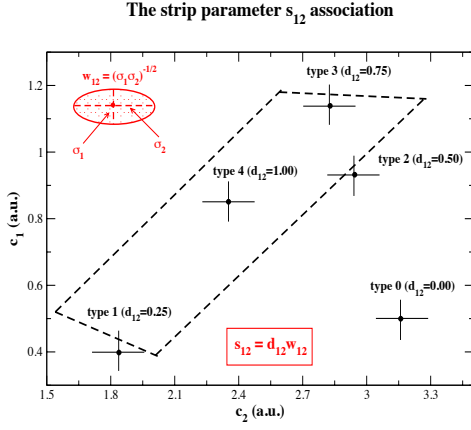
Fig. 7.— The schematic view of the strip parametrization in the example of the c_1-c_2 2D projection in arbitrary units (a.u.). We report the method described in Section 2.4 to assign to each point of the 2D projection of the WGS a value of the *discrete strip parameter d_{12}* and the associated value of the *weight strip parameter w_{12}*. The combination of these two values provides the *continuos strip parameter s_{12}* for each given source (see Equation 1).
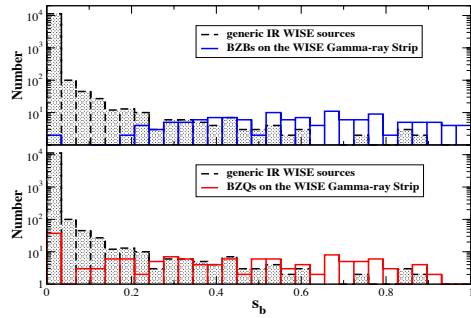
Fig. 8.— The distribution of the strip parameter s_b for the BZBs (blue) and the BZQs (red) that lie on the WGS in comparison with the generic IR *WISE* sources (black).
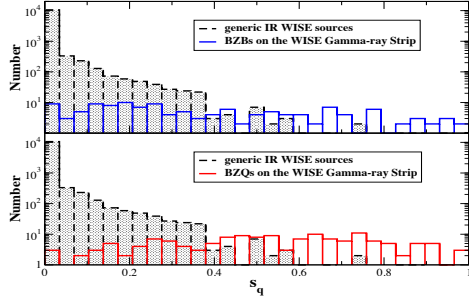
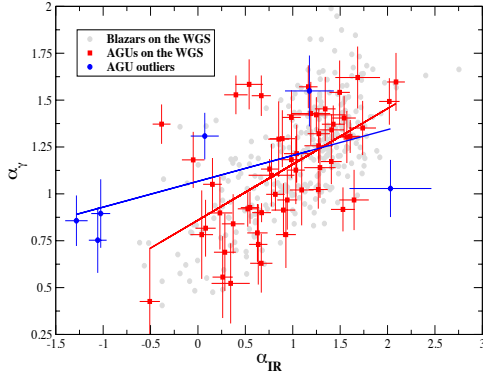Fig. 9.— Same of Figure 8 for the distribution of the s_q parameter.

Fig. 10.— The correlation between α_{IR} and α_γ for the *WISE* counterparts of the AGUs. The background grey circles represent the correlation found for the WGS blazars (see Paper II), while the red filled squares are the AGUs that have been found consistent with the WGS accordingly with our parametrization. The remaining 6 outliers (blue filled circles) show a weaker and different correlation than the other samples.
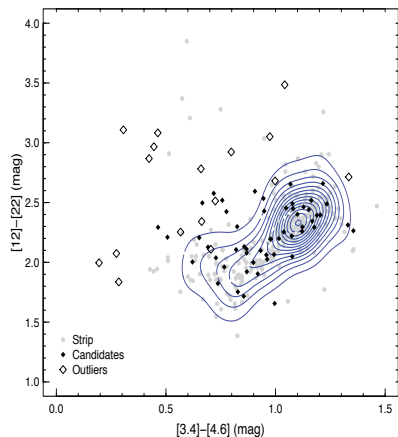
Fig. 11.— The isodensity contours drawn from the KDE technique for the blazars of the WGS (grey circles) are shown for the case of the [3.4]-[4.6]-[12]-[22] μm 2D projection. The AGU identified as blazar candidates (filled black squares) are also shown in comparison with the outliers (black open square) to show the consistency between the WGS parametrization and the KDE analysis.
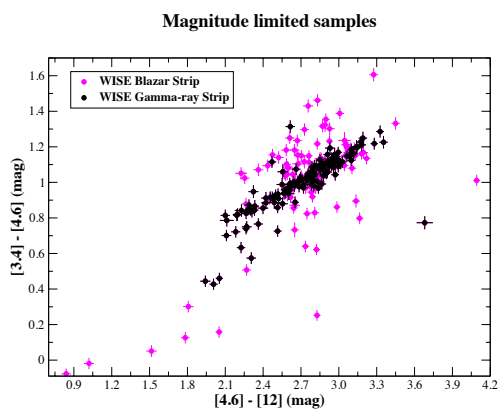

Fig. 12.— The 2D projection of the *WISE* Blazar Strip (magenta) and the subregion of the WGS (black) in the IR color diagram [3.4]-[4.6]-[12] μm when only bright IR blazars are considered (i.e., those with *WISE* magnitudes in the ranges: $m_1 \leq 13.5$, $m_2 \leq 12$, $m_3 \leq 11$, $m_4 \leq 7.5$, respctively).
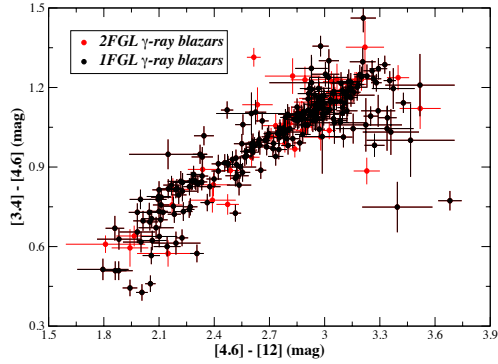
Fig. 13.— The 2D projection of the WGS in the IR color diagram [3.4]-[4.6]-[12] μm when only bright γ-ray blazars listed in the 1FGL (black) are considered in comparison with those in the 2FGL (red). There are no clear differences on the thickness of the WGS in this 2D projection due to the different samples considered.